A scalable label-free approach to separate human pluripotent cells from differentiated derivatives

N. A. Willoughby,[1,a),b)] H. Bock,[2,a)] M. A. Hoeve,[3] S. Pells,[3] C. Williams,[1,c)] G. McPhee,[1,d)] P. Freile,[3] D. Choudhury,[1] and P. A. De Sousa[3,b)]
[1]*Institute for Biological Chemistry, Biophysics and Bioengineering, School of Engineering and Physical Sciences, Heriot-Watt University, Edinburgh EH14 4AS, United Kingdom*
[2]*Institute for Chemical Sciences, School of Engineering and Physical Sciences, Heriot-Watt University, Edinburgh, United Kingdom*
[3]*Centers for Clinical Brain Sciences and Regenerative Medicine, University of Edinburgh, Edinburgh EH16 4SB, United Kingdom*

(Received 9 December 2015; accepted 1 January 2016; published online 14 January 2016)

The broad capacity of pluripotent human embryonic stem cells (hESC) to grow and differentiate demands the development of rapid, scalable, and label-free methods to separate living cell populations for clinical and industrial applications. Here, we identify differences in cell stiffness, expressed as cell elastic modulus (CEM), for hESC versus mesenchymal progenitors, osteoblast-like derivatives, and fibroblasts using atomic force microscopy and data processing algorithms to characterize the stiffness of cell populations. Undifferentiated hESC exhibited a range of CEMs whose median was nearly three-fold lower than those of differentiated cells, information we exploited to develop a label-free separation device based on the principles of tangential flow filtration. To test the device's utility, we segregated hESC mixed with fibroblasts and hESC-mesenchymal progenitors induced to undergo osteogenic differentiation. The device permitted a throughput of 10^6–10^7 cells per min and up to 50% removal of specific cell types per single pass. The level of enrichment and depletion of soft, pluripotent hESC in the respective channels was found to rise with increasing stiffness of the differentiating cells, suggesting CEM can serve as a major discriminator. Our results demonstrate the principle of a scalable, label-free, solution for separation of heterogeneous cell populations deriving from human pluripotent stem cells.
[http://dx.doi.org/10.1063/1.4939946]

INTRODUCTION

Stem cell research and regenerative medical treatments are progressing towards the development of more complex, cell-based, advanced therapies as an alternative to the use of therapeutic proteins. Bio-production and processing of these cell-based products for the clinic, however, necessitate a re-think of current manufacturing technology. An important aspect in the manufacturing of any medicinal product is control of the composition of matter to assure its efficacy and reproducibility of outcomes following its use. This will be especially critical for the manufacture of stem cell derived cellular products given the potential of the starting cellular resource to differentiate in uncontrolled manner or contaminate the final end product. This applies to end products used *in vitro*, such as in high-throughput screening platforms, as well as

[a)]N. A. Willoughby and H. Bock contributed equally to this work.
[b)]Authors to whom correspondence should be addressed. Electronic addresses: N.A.Willoughby@hw.ac.uk, Tel.: +44 131 451 4377, Fax: +44 131 451 3129 and paul.desousa@ed.ac.uk, Tel.: +44 131 242 6646, Fax: +44 131 242 6201.
[c)]Current address: School of Materials, University of Manchester, Manchester, United Kingdom.
[d)]Current address: ARC Centre of Excellence in Convergent Bio-Nano Science and Technology, Mawson Institute, University of South Australia, Adelaide, Australia.

for *in vivo*, for cell engraftment to treat degenerative disease or damaged tissues. The broad capacity of human pluripotent stem cells, as derived from embryos or induced by genetic manipulation of adult cells, accentuates concern for their usage as source material for the latter, owing to the risk of a contaminating undifferentiated cell giving rise to benign tumours of differentiating cells (i.e., teratomas), or malignant metastatic tumours composed of highly proliferative cells (i.e., teratocarcinoma). Knowledge and control of the composition of stem cell derived cell products may also be important to achieve specific therapeutic outcomes, as evidenced recently by Van Vliet and coworkers who reported that different subpopulations within culture expanded bone marrow-derived mesenchymal stromal cells possess unique tissue regenerative potential (Lee *et al.*, 2014).

The majority of scalable purification processes used in the production of therapeutic proteins by the pharmaceutical industry are based on the use of column chromatography to obtain the desired levels of purity. However, traditional absorption-based column chromatographic techniques are unlikely to be applicable to cell purification due to the greater size, sensitivity, and complexity of cells compared to proteins. Currently, the most commonly applied approach to cell purification in life sciences and small scale clinical applications is largely dependent on the recognition and selection of cell surface ligands, as commonly achieved by flow cytometric- or magnetic bead-based sorting. However, these methods are severely constrained by a requirement for cell-specific ligands (i.e., knowledge, availability, and specificity thereof) and the availability of complementary probes. Moreover, probes likely remain associated with the cell and/or cell preparation after segregation, the consequences of which are not known, but are generally recognized to risk invoking immune or toxic responses in patients. Importantly, these ligand-based methods are limited in their throughput, and in their current form do not constitute scalable strategies to purify the anticipated cell numbers for pluripotent stem cell-based therapeutic products.

The predicted future reliance of health care on advanced therapy medicinal products (ATMPs), the new category of "drugs" that are actually cell populations, will create demand for large-scale cell separation embedded in automated cell culture production platforms. Worldwide, hundreds of cell-based clinical trials are proposed and currently ongoing (as searchable on the USA National Institutes of Health clinical trials registry www.clinicaltrials.gov, or the European counterpart www.clinicaltrialsregister.eu), which, once demonstrated successful and safe, will warrant production of large quantities of cells according to Good Manufacturing Practice. In the manufacture of cells for therapy, the current most commonly used large-scale cell separation in method applied in the context of blood products makes use of biophysical cell parameters and selects cells on the basis of size and density by means of density gradient centrifugation. This method is most effective when considering cells of distinctly different densities such as separating enucleated red blood cells from white blood cells. Moreover, though centrifugation itself is a relatively easily scaled unit operation, scale-up requires a transition from semi-batch to continuous operation, an operating mode not easily compatible with density gradients. In addition, physical shear forces on the cells increase as the size of the device increases, risking damaging sensitive cell products. Thus, there is an urgent need for new cell separation methods that lend themselves to large-scale use for clinical cell manufacture.

New, alternative cell separation technologies on the basis of biophysical properties have recently been reported which potentially offer opportunities for a passive (i.e., without exerting an external force on the cells) and label-free sorting technique (reviewed in Bhagat *et al.*, 2010; Gonzalez-Gonzalez *et al.*, 2012; Darling and Di Carlo, 2015; and Kunze *et al.*, 2015). Many of these technologies are based on multiple parameters, often including size, and one or more of additional properties including density, shape, hydrophobicity, net charge, sedimentation density, intrinsic hydrodynamic forces, differential magnetic susceptibility of cell (-content), refractive index, polarisability, membrane properties such as surface charge, cytosol conductivity, and cell deformability/stiffness. These technologies have mainly been designed as microfluidic devices, only suitable for small-scale separation. The aim of this study was to develop a novel alternative to absorption-based and label-requiring selection methods for stem and derivative cells that is readily scalable and could be broadly implemented in industrial and therapeutic applications. Using atomic force microscopy (AFM), we identified variations in cell stiffness related to

cell phenotype and could identify optimum stages at which pluripotent human embryonic stem cells (hESC) could be separated from their progeny. Using a separation device based on the principles of tangential flow filtration (TFF), we demonstrate the proof-of-principle ability to scalably and selectively enrich or deplete for particular cell populations primarily on the basis of knowledge of cell stiffness, without reliance on cell labeling with high-affinity probes for cell specific antigens. Our findings underpin the development of a novel cell-bioprocessing platform to meet the future needs of pluripotent stem cell manufacturing for industrial and clinical applications.

MATERIALS AND METHODS

Cell culture and differentiation

The use of hESC lines in this project was approved by the Medical Research Council (MRC) steering committee overseeing the UK Stem Cell Bank. H1-hESCs were licensed from WiCell (available from the Wisconsin International Stem Cell Bank (www.wicell.org)). To facilitate recognition of cells with an active pluripotency promoter, for some experiments, a transgenic clone of H1-hESC was used where expression of Green Fluorescent Protein is directly linked to a pluripotency associated promoter (Oct4; H1-Oct4-EGFP cells, WiCell) (Gerrard *et al.*, 2005). Starting hESC populations used in this study were at passage 60–70. All hESCs were cultured under feeder-independent conditions in mTeSR1 medium (STEMCELL Technologies) containing 50 U/ml penicillin, 50 μg/ml streptomycin, and 2.5 μg/ml Fungizone at 37 °C, 5% CO_2 in air. Undifferentiated hESCs were grown on Matrigel^{TM} (Becton Dickinson) and routinely passaged by mechanical scraping following treatment with collagenase IV (200 u/ml in Knockout Dulbecco's Modified Eagle Medium (DMEM)). hESC cultures were seeded at a density of approximately 100 000 cells/cm^2 and split at a pre- to post-plating ratio of 1:2 wells (i.e., passaging cells from one well into two new wells). hESC cultures were passaged at ∼80% confluence every 4–5 days. Addition of G418 to culture medium (1:1000) allowed selective ablation of Oct4-EGFP transgene silenced cells, while visual inspection was employed to correlate GFP expression with undifferentiated hESC colony morphology. Human dermal fibroblasts (HDFs) from neonatal foreskin (Cascade Biologics) were cultured on plastic (Corning), in M106 medium (Invitrogen) supplemented with low serum growth supplement (LSGS, 50×), at 37 °C, 5% CO_2 in air.

H1-hESCs were differentiated to a mesenchymal progenitor phenotype (designated hESC-MP) as reflected by flow cytometric determination of negativity for CD14 and CD34 and detection of CD105, CD90, CD73, and Stro1, using a method previously developed and validated by ourselves and others ((De Sousa, 2006; Harkness *et al.*, 2011; and Velugotla *et al.*, 2012). The method involves plating hESCs (5×10^5 cells/9.6 cm^2) on hyaluronan (HA; also known as hyaluronic acid or hyaluronate) (1200 kD; Calbiochem Cat Nr 385908) in a medium that would otherwise support hESC self-renewal (human dermal fibroblast conditioned medium (HDF-CM) composed of KO-DMEM, 20% Knockout serum replacement (KOSR, Invitrogen), 1 mM glutamine, 0.1 mM β-mercaptoethanol, and 4 ng/ml bFGF). An HA stock solution for tissue culture plate coating was produced by solubilizing HA in Phosphate Buffered Saline (PBS) at 10 mg/ml Wells were coated with this HA stock solution at 0.1 ml/cm^2 for 30 min at 4 °C, and plates warmed to room temperature prior to cell plating. Cells were passaged every 5–7 days by collagenase IV treatment and scraping, as described above. After ∼10 passages on HA, cells had irreversibly adopted the hESC-MP phenotype.

For osteogenic differentiation of hESC, H1-hESCs were steered towards the mesenchymal progenitor phenotype hESC-MP as described above, and then gradually transitioned over 4 days from the HDF-CM medium to 100% STEMPRO® MSC SFM medium (Life Technology) by exchange of media mixed in different ratios (100:0; 75:25; 50:50; 25:75, 0:100) at daily intervals. Differentiation of hESC-MP cells towards osteoblasts was carried out on cell culture plates coated with HA using the StemPro Osteogenesis Differentiation Kit (Life Technology), according to manufacturer's instructions. hESC-MPs cultured in STEMPRO MSC SFM medium served as negative control. Differentiation lasted 21 days, re-feeding every 2–3 days and passaging every 5–7 days.

ATOMIC FORCE MICROSCOPY

Cell stiffness was probed by force spectroscopy, i.e., by measuring force versus indentation curves using AFM (see supplementary material). Subsequent quantitative characterization of cell stiffness was achieved by fitting the proper form of the Hertz equation (Hertz and Angew, 1881) to the repulsive indentation part of these curves (Kuznetsova *et al.*, 2002 and Radmacher, 1992). The indentations formed rectangular arrays with pixel sizes between 1 and 18 μm^2. Indentation speed was 10 μm/s for both tip approach and retraction at a maximum indentation force of ~2 nN. Typically, all force spectroscopy was completed in approximately 4–5 min for each array. Each force versus indentation curve was analyzed using an in-house procedure (see supplementary material), which provided a cell elastic modulus (CEM) value to characterize the local stiffness of the sample, with low CEM equaling low sample stiffness and high CEM equaling high sample stiffness. Analysis of all force versus indentation curves and subsequent algorithm application (see supplementary material) resulted in CEM-maps such as the one shown in Fig. 1(a), and CEM probability distributions such as those shown in Figures 1(b) and S1 in the supplementary material. Typically, several thousand indentations were performed per biological sample of which up to 1000 passed the quality test and were used for further analyses. Per biological sample, multiple CEM-maps were produced, from different individual cells and/or from cells in a confluent monolayer, typically stemming from more than one well.

Micromesh-based cell separation

A scalable TFF device was produced from stainless steel and consisted of two mirror-symmetric blocks of steel with S-shaped semicircular channels machined to a depth of 1 mm into the surface (Fig. 2). The shape of the channel was designed to maximize length and therefore separation area of the device within the manufacturing and assembly constraints of our facilities. The blocks were bolted together, separated by 8 μm nylon micromesh of approximate thickness 10 μm and relative porosity of 0.27 (estimated in both cases from microscopy images) (MicroSieves^{TM}, BioDesign Inc., Carmel, NY), resulting in a cylindrical channel, 7 cm in length, divided into two by mesh. The mesh division created the equivalent of channels 1 and 2 in our previously fabricated Microchannel Separation Device (MSD) (supplementary material, Fig. S2 and Choudhury *et al.*, 2012), with flow and pressure driving forces across the mesh controlled by adjusting the liquid flow rates above and below the mesh using microprocessor-controlled pumps. The channel "above" the mesh is equivalent to a traditional TFF retentate flow and the channel "below" equivalent to permeate. The dimensions of this device gave an effective separation area of 1.4 cm^2, with a maximum possible linear fluid velocity within the channel of 15 cm/s, constrained by the pumps used. Flow rate conditions were chosen at 1.5 ml/min into the device (channel 1, upper left input in Fig. 2(b)) with the flowrate into the lower left input of channel 2 held at 0 ml/min and the lower right output of channel 2 controlled at 0.4 ml/min. This resulted in a retentate flow (upper right output, channel 1, Fig. 2(b)) of 1.1 ml/min and a permeate volumetric flux (lower right channel, Fig. 2(b)) of 0.4 ml/min. These numbers were chosen based upon trial and error to provide reasonable retentate and permeate flow rates to encourage any separation. Ideally, such a device would be controlled by pressure drop across the membrane alone rather than flow rate, however this was not possible in the current design. The flow rates chosen give a linear liquid velocity of 6.5 cm/s above the membrane and 1.7 cm/s below the membrane, respectively, resulting in Reynolds numbers of 40 above and 11 below.

Cell separation

For all cell types, single cell suspensions were prepared using TrypLE^{TM} Express (Life Technologies) and cell numbers quantified by hemocytometer. For cell separation experiments, different cell populations were pooled in particular cell ratios to obtain an overall cell concentration of approximately 1×10^6 cells/ml. Samples of feed material, permeate (that which has passed through the mesh into an outlet channel), and retentate (that which remains in the main channel) were collected for analysis. Flow rates through the mesh-based separation device

A

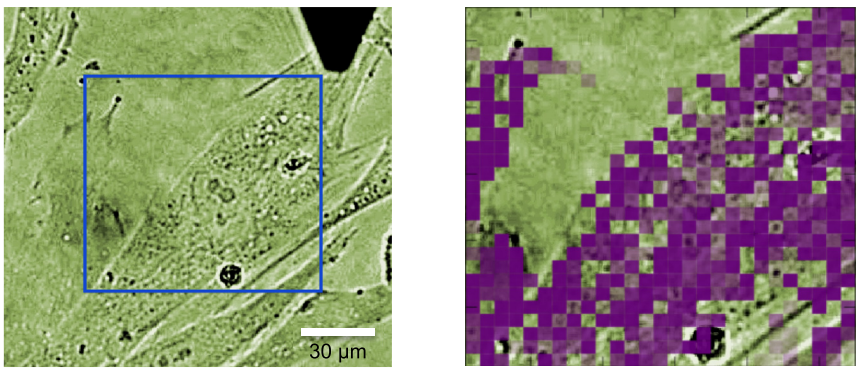

B

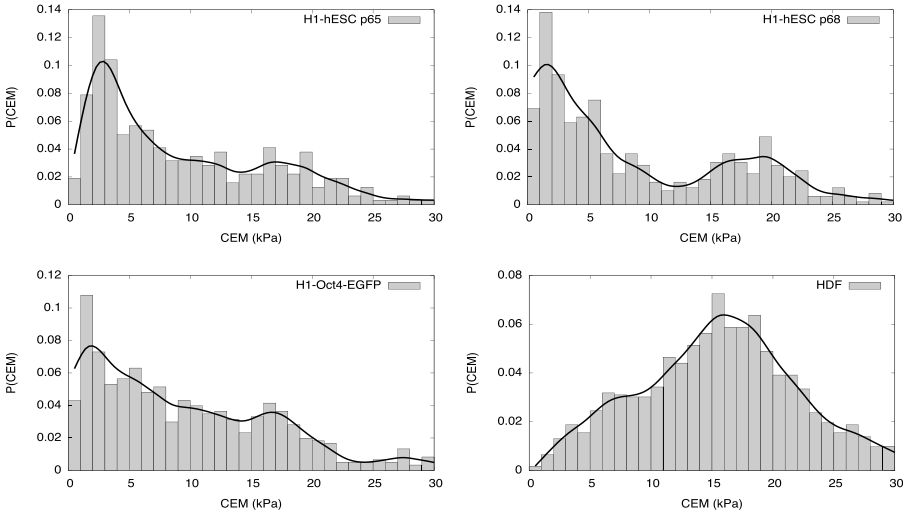

C

Cell type	Nr of points included	Median CEM (kPa)
H1-hESC p65	299	6.37
H1-hESC p68	473	5.88
H1-Oct4-EGFP	527	6.77
HDF	1154	15.51

FIG. 1. Characterisation of cell stiffness for hESC and differentiated progeny using atomic force microscopy. Per cell type, thousands of force versus indentation curves were acquired and analyzed by means of a computational analysis algorithm (see supplementary material), ultimately providing a CEM (in kPa) value to characterize the stiffness of the cell population. (a) Analysis (see supplementary material) of all force versus indentation curves resulted in elasticity CEM-maps such as the one shown in the panel on the right-hand side, which is overlaid on an HDF cell preparation image on the left-hand side. For each small square on the CEM-map, one force-indentation curve was measured in the center of the square. The resulting color of the square represents the measured CEM value, i.e., stiffness, with darker colors indicating higher stiffness. (b) Probability distributions of CEMs (as P(CEM)) generated through ordering the measured CEM values into bins of equal width of 0.5 kPa. (c) Number of high-quality force-indentation curves used to extract CEM values and the median CEM (in kPa) for the various cell types.

(MBSD) were maintained at 1.5 ml/min in channel 1 (above the mesh; retentate) and 0.4 ml/min in channel 2 (below the mesh; permeate) at all times. In each experiment, a 5 ml suspension of cells in PBS (pH 7.2) was separated using the MBSD. As an example, cells in an approximate 1:1 mixture of hESCs and HDFs were at a total cell concentration of 0.96×10^6 cells/ml (range 0.8–1.1×10^6 cells/ml, $n = 9$ measurements from 3 runs). After the 5 ml of cells were passed through the device, a further 5 ml of PBS was pumped into the feed inlet of the device to wash out any cells remaining in the channels into the retentate and permeate.

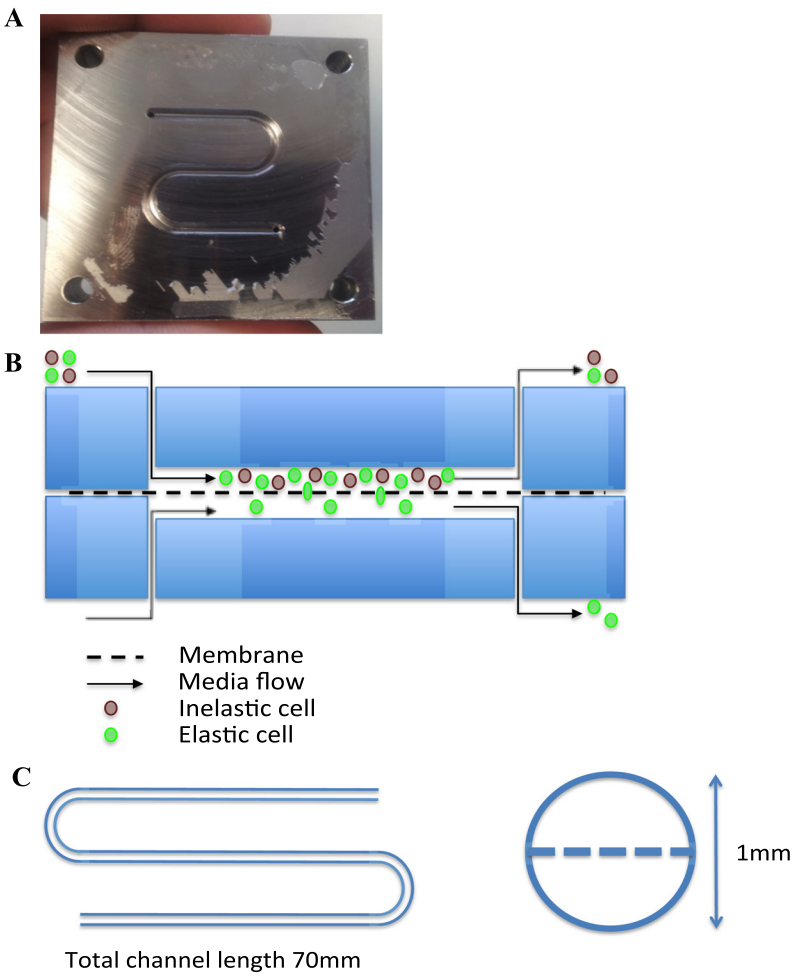

FIG. 2. Mesh-based separation device (MBSD). (a) Photograph of the S-shaped flow channel inside the MBSD after removal of the mesh and top-half of the device. (b) Schematic of operation of the device drawn in vertical position, indicating the inlets for feed population (upper left) and medium (lower left), and outlets for the purified population (retentate, upper right) and sorted population (permeate, lower right), in relation to the mesh dividing the channel. (c) Schematic of the flow layout as duplicated in the top of and bottom half of the device, along with a channel cross section showing membrane position.

Flow cytometry

Flow cytometry was performed on a FACSCalibur (Becton Dickinson) to assess cell type representation within heterogeneous cell samples before and after separation. For the hESC/HDF separation experiments, HDF were discriminated from hESCs using an antibody to CD13 (APC-conjugated mouse anti-human CD13, BD Pharmingen™; 1:1000 dilution) (Kahler *et al.*, 2013) and an appropriate isotype control. Depletion calculations were based on changes in numbers of CD13-positive cells in the various cell samples (feed, permeate, and retentate) following separations. For the hESC/osteoblast separation experiments, the pluripotency associated surface marker TRA-1-60 (PE-conjugated mouse anti-human TRA-1-60-R; Biolegend®; 1:1000) and an appropriate isotype control were used to identify hESCs, and osteoblast enrichment calculations were based on changes in numbers of TRA-1-60 positive cells in feed and retentate.

Alizarin red staining

At various time points during differentiation of hESC-MP towards osteoblasts (days 1, 6, 11, 15, and 21), Alizarin red staining was used to assess the presence of calcium deposits. Cells

cultured in mTeSR1 medium (negative control) or under osteogenic differentiation conditions on HA were washed twice with PBS, fixed with 95% methanol at room temperature, and stained with Alizarin red S (10 mg/ml) (Sigma) (10 min, pH 4.2). After washing with water, wells were inspected using light microscopy, and images taken for qualitative examination.

RESULTS

Assessment of cell stiffness using atomic force microscopy

Recently, we identified differences in cell stiffness between undifferentiated pluripotent hESCs and terminally differentiated cells (HDFs) following measurements of limited samples of cells by AFM (Kiss *et al.*, 2011). Here, we first sought to compare stiffness of these two cell types with that of hESC-MP cells as a surrogate intermediate cell type.

AFM measurements to determine stiffness (see Fig. 1 and supplementary material) were carried out on individual cells of the following populations: an undifferentiated hESC line (H1-hESC; at two different passage numbers, p65 and p68), a transgenic subclone of H1-hESC containing a GFP reporter (H1-Oct4-EGFP cells), H1-hESC differentiated to a mesenchymal progenitor (hESC-MP), and HDFs sourced from neonatal foreskin. For each cell type, several thousand force versus indentation curves were acquired and analyzed (see supplementary material). This analysis resulted in CEM-maps such as the one shown in Fig. 1(a). Next, probability distributions of CEMs were determined by ordering the data into bins of equal width of 0.5 kPa (Fig. 1(b) and supplementary material), ultimately providing a median CEM value (in kPa) to characterize the stiffness of a given cell population (Fig. 1(c)), with a low CEM indicating low stiffness and high CEM indicating high stiffness. Our data show that median CEMs of fully differentiated cells are on average nearly three-fold higher than those of pluripotent (undifferentiated) stem cells (i.e., differentiated cells are approximately three times as stiff) (Fig. 1(c)).

Stiffness-based cell separation

Although some degree of difference in median CEM between the cell types was anticipated (Butt *et al.*, 2005 and Kiss *et al.*, 2011), the observed magnitudes offered the potential of using elastic modulus as a cell separation tool for cells that are undifferentiated, terminally differentiated, or in an intermediate state. To exploit this idea, we developed stiffness-based cell separation techniques to test feasibility. Previous efforts from our group had yielded a microfluidic cell selection device containing 8 μm wide channels (Choudhury *et al.*, 2012). Based on optical observation, this channel width was seen to reject most mammalian cells, presumably on a size basis. However, preliminary experimental trials with the microfluidic device that involved qualitative monitoring of hESCs and HDFs via phase contrast and fluorescence microscopy showed that cells with a sufficiently high degree of flexibility (i.e., a low CEM) were able to pass through the separating channels to end up in the flow-through sample. To investigate this in more detail, we developed our previously designed microfluidic separator further and fabricated a MSD (Fig. S2 in the supplementary material) to ascertain the optimal design. Though the MSD was able to separate mixed cell populations, due to size constraints this device only allowed selection of a relatively small number of cells per run, precluding accurate quantification of separation efficiency by means of flow cytometry. Analysis of separation was therefore carried out by comparative optical and fluorescent microscopy, after flowing an approximate 50:50 mixture of fluorescent H1-Oct4-EGFP hESCs and HDFs into the device. Using our device to separate cells in this model system allowed us to observe Oct4-EGFP cells passing readily through the narrow separating channels into channel 2 under green fluorescent illumination, while the stiffer HDFs (higher CEM) remained in channel 1 (data not shown). Whilst comparison of videos under fluorescent and phase contrast conditions indicated efficient separation, our inability to simultaneously video under fluorescence and phase contrast precluded direct quantification of separation efficiency.

Micromesh-based cell separation

We next developed the MSD further into a larger, scalable, tangential flow cell separation device. This new, MBSD was able to efficiently and accurately separate heterogeneous cell populations (feed population; example average cell concentration 0.96×10^6 cells/ml (range $0.8–1.1 \times 10^6$ cells/ml, n = 9 measurements from 3 runs) into two distinct populations, namely, a population enriched for cells unable to pass through the mesh (the "retentate"; example average cell concentration 0.82×10^6 cells/ml (range $0.77–0.92 \times 10^6$ cells/ml, n = 9 measurements from 3 runs)) and a sorted population that separated from the former by passing through the mesh (the "permeate"; example cell concentration 0.55×10^6 cells/ml (range $0.53–0.57 \times 10^6$ cells/ml, n = 9 measurements from 3 runs)). We have previously shown that cells passing through microchannels of this size remain viable (as measured by propidium iodide and thiazole orange comparative flow cytometry) (Choudhury *et al.*, 2012). Figure 3 is a representative example of flow cytometric analysis of feed, permeate, and retentate material corresponding to the example data quoted above, showing that these three populations have a similar size profile in Forward Scatter ((X-Axis; FSC)/side scatter (Y-Axis; SSC) dot plots, with FSC proportional to cell size and SSC proportional to cell granularity/complexity (Figure 3, left column). After running a mixture of H1-Oct4-EGFP cells and CD13-labelled HDFs through the MBSD, the permeate contained considerably fewer HDFs compared to the feed population. HDFs were reduced from 53.9% (range 51.0%–55.9%) in the feed population to 31.3% (range 31.1%–31.4%) in the permeate (n = 9 measurements from 3 runs) (exemplified by the contour diagrams in Fig. 3, middle column). Conversely, the proportion of HDFs increased to 63.2% (range 61.1%–64.1%) in the retentate (n = 9 measurements from 3 runs) (exemplified in Fig. 3, contour diagrams). Our flow cytometry data indicate that the passage of hESCs through the membrane is relatively unhindered, whilst HDFs are preferentially excluded. Overall loss of cell number (based on total cell balance) in the device was negligible (total cells in feed: $4.0–5.5 \times 10^6$; total cells in retentate: $4.0–4.8 \times 10^6$; total cells in permeate: $0.93–1.0 \times 10^6$ (Fig. 3(d)); overall balance $\geq 100\%$, likely due to clumps of cells separating into single cells in the device and slightly artificially inflating counts). Based on total cell numbers of each cell type in the feed and the permeate, the separation shown in Fig. 3 represents a 44% relative reduction in the permeate of the percentage of HDFs present in relation to H1-Oct4-EGFP cells following a single pass, as calculated using the formula below:

$$\left(\frac{Percentage\,HDF\,in\,Feed - Percentage\,HDF\,in\,Permeate}{Percentage\,HDF\,in\,Feed}\right) \times 100.$$

Experimental repeats consistently showed HDF removal of around 40% in a single pass for the model H1-Oct4-EGFP/HDF cell system (range: 38.1%–44.4%; n = 9 samples from 3 runs). Flow control enabled a relative 3:1 split in favor of the retentate in terms of volumetric flow rate to ensure a pressure driving force across the membrane encouraging permeate flow. As this device design did not include features for increasing turbulence and pressure-driving force as would be seen in a traditional TFF cassette, there is considerable scope for further improvement of separation efficiency and increased permeate flow rates relative to retentate flow. Importantly, plotting the live gated cells as overlay FSC/SSC dot plots, with CD13-APC cells in red (HDF) and Oct-4GFP cells in green (H1-Oct4 cells), shows enrichment/depletion of specific cell types in permeate and retentate without a change in size distribution profile (Fig. 3, the right column).

Cell stiffness during osteoblast differentiation

Using our MBSD, we were thus able to separate heterogeneous cell populations into distinct populations based on CEM. To demonstrate that cell stiffness constitutes a reliable biophysical attribute varying with cell differentiation state of the same cell type, we next tried to separate cells at various stages as they were being differentiated from their own progenitors. For this, we used the well-established practice of directing osteogenesis of mesenchymal stem

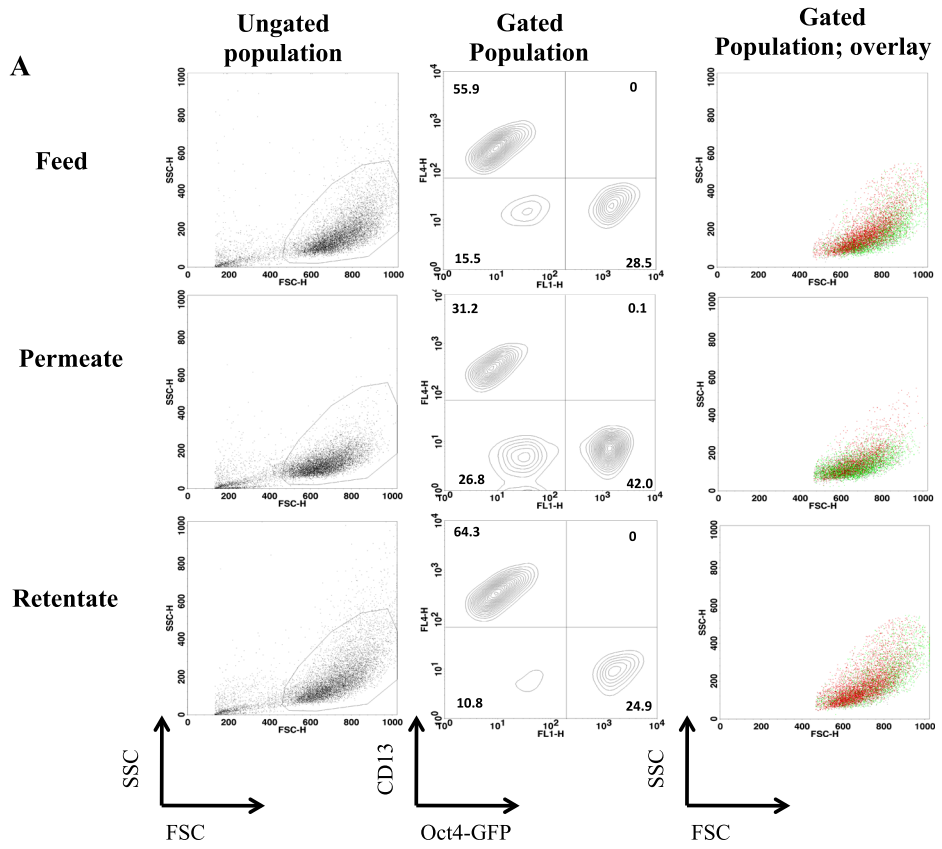

B

Sample	Feed	Permeate	Retentate
UL	55.9	31.2	64.3
UR	0	0.1	0
LL	15.5	26.8	10.8
LR	28.5	42.0	24.9
% HDF change	n/a	-44%	+15%

FIG. 3. Flow cytometric analysis of cells separated with MBSD. (a) In the left column, flow cytometric analysis of 5 ml of a 1:1 mixed population of H1-Oct4-EGFP cells and HDFs prior to separation (feed; top row) and following a single pass through the MBSD (permeate cells; middle row, and retentate cells; bottom row) shows similarly sized populations in forward scatter (X-Axis; FSC)/side scatter (Y-Axis; SSC) dot plots, with FSC proportional to cell size and SSC proportional to cell granularity/complexity. In the middle column, gated live cells of these three cell populations have been plotted as contour diagrams, with CD13-APC on the Y-Axis (HDFs) and Oct4-GFP on the X-axis (H1-Oct4-EGFP+ cells). These plots show that a typical single pass cell separation resulted in a reduction of HDFs (in upper left quadrants) in permeate compared to feed population from 55.9% to 31.2%, with a concurrent increase in HDFs in the retentate to 64.3%. Contour lines in the four quadrants represent CD13-positive/Oct4-negative cells (upper left), Oct4-positive/CD13-positive cells (upper right), Oct4-negative/CD13-negative cells (lower left), and Oct4 positive/CD13 negative cells (lower right). In the right column, FSC/SSC dot plots of the live gated cells represent overlays of CD13-APC cells in red and Oct-4GFP cells in green, showing enrichment/depletion of specific cell types in permeate and retentate without a change in size distribution profile. (b) Tabulation of data presented in the middle column above, summarizing the reduction in HDF cells in permeate compared to feed population from 55.9% to 31.2%—i.e., a 44% relative reduction, with a concurrent increase in HDFs in the retentate to 64.3%—i.e., a 15% relative increase. Figures and table depict a representative example of 3 independent separation experiments.

cells using a cocktail of reagents (Sottile *et al.*, 2003). Osteogenic differentiation was carried out with our mesenchymal-like cells hESC-MP over 21 days, with cell samples taken at regular time points for Alizarin red staining to assess calcium content as proxy for cell mineralization, and for AFM analyses to assess cell stiffness (Figs. 4 and S1 in the supplementary material).

The probability distribution curves in Figures 4 and S1 (supplementary material) illustrate the typical variation in CEM as measured during differentiation of hESC-MPs towards

osteoblasts. The general trend shows an increase in sample CEM during the early stages of differentiation, i.e., an increase in cell stiffness. This is followed by a decrease in sample CEM (i.e., a decrease in cell stiffness) between days 11 and 15, before another sharp increase in CEM is observed at day 21. Thus, the median sample CEM appears to vary non-monotonously during the differentiation process (Fig. 5). Interestingly, the CEM distribution at day 11 is bimodal with the two probability maxima corresponding to those of day 6 and 15, respectively. This may indicate that at this stage the cells transform relatively rapidly into a softer state. By day 15, essentially all cells seem to have reached this state. The CEM distribution at day 21 is likewise bimodal with the probability maximum at lower CEM corresponding to the single maximum of the day-15 CEM distribution. The origin of the probability maximum at higher CEM is less clear. Alizarin red staining performed in parallel indicates increasing levels of mineralization in the culture wells over time (Fig. 4). By day 21, the majority of the cells had become heavily mineralized. In addition, crystals could be observed in the wells, which made the AFM difficult and may also have contributed to the stiffer responses. The lack of any population of "stiff" cells at day 15 as identified by the CEM data indicates that the level of mineralization does not offer a complete explanation for the bimodal distribution at day 21, and suggests that the cells may in fact become softer in advance of mineralization, perhaps for flexibility or mobility reasons.

Separating osteoblasts from their precursor hESC-MPs using MBSD

The use of hESC-MP-derived osteogenic derivatives for reconstruction of bone constitutes a clinical exemplar of a therapeutic approach requiring scaled production of cells and purification thereof, which at present do not exist. To test MBSD's utility for therapeutic cell

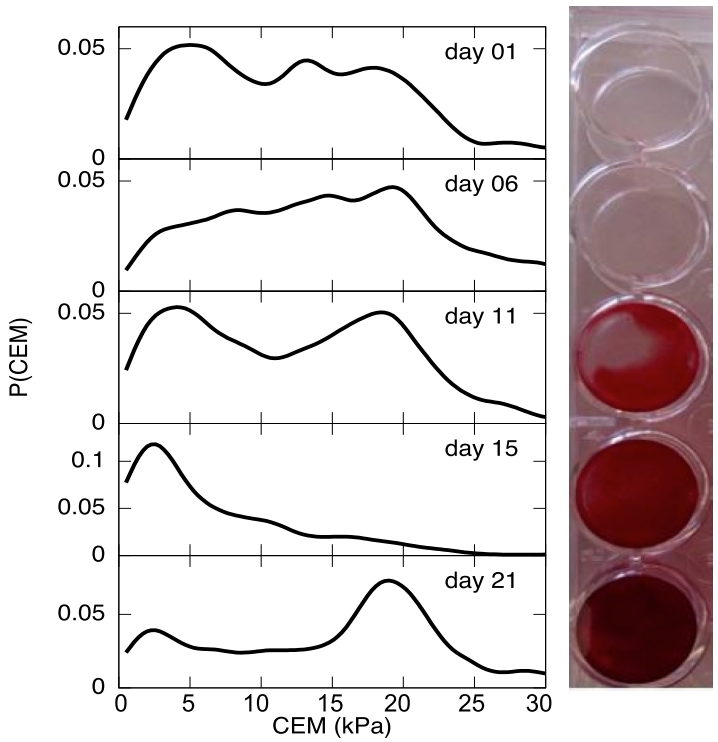

FIG. 4. Alizarin red staining and CEM probability distributions of hESCs undergoing osteogenic differentiation. hESC-MP cells cultured in plates coated with Hyaluronan in medium supporting osteogenic differentiation show increasing calcification over the course of differentiation, as assessed by alizarin red staining on the indicated days following the start of differentiation (D1-6-11-15-21; photograph of stained wells on the right hand side). Cell presence in all wells was confirmed by microscopic examination and subsequent stiffness measurements and sample imaging performed with AFM (data not shown). Continuous probability distributions of CEM (P(CEM)) plotted against CEM in kPa (see supplementary material) for the corresponding days are shown in the graphs to the left of the stained wells. The distributions demonstrate the presence of populations with higher CEM (i.e., higher stiffness) at day 6, 11, and 21.

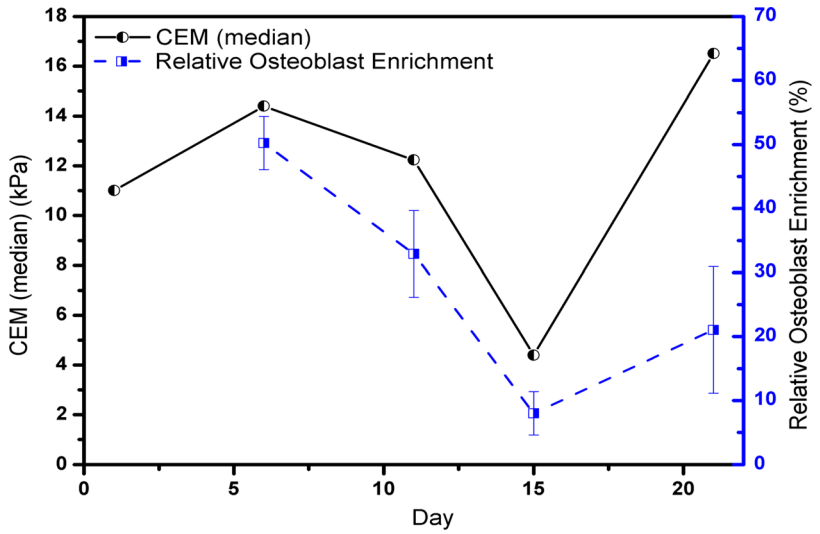

FIG. 5. CEM versus cell separation achievement over the course of hESC osteogenesis. Variations in median CEM (in kPa; Y-axis on the left) of hESC-MP cells undergoing osteogenesis, as measured at various time points post initiation of differentiation (on X-axis), are plotted in relation to relative enrichment (in %; right Y-axis) of pluripotent hESCs achieved in the retentate after running 5 ml of an hESC/osteoblast mixed cell population through the MBSD device once at the indicated days during differentiation. Over time, the cells' stiffness increases, peaking at day 6 (high kPa), after which the median CEM indicates a lower sample stiffness (day 11), and average low stiffness comparable with that of hESC at day 15. Enrichment calculations are based on changes in the numbers of cells expressing pluripotency marker TRA-1-60 in feed and permeate, with bars indicating the extent of dataset range. From day 1 till day 15, stiffness corresponds with enrichment, in that higher stiffness of the osteoblasts mixed in with the hESC resulted in higher enrichment of the soft hESCs in the permeate.

production, we collected hESC osteolineage derivatives at various days post-initiation of differentiation and mixed them 1:1 with TRA-1-60-R-PE-labelled hESCs for subsequent separation, analogous to our hESC/HDF experiments (feed population; example average cell concentration 1.19×10^6 cells/ml (range 1.14–1.22×10^6 cells/ml, n = 3 measurements of single-pass separation); retentate; example average cell concentration 0.73×10^6 cells/ml (range 0.67–0.83×10^6 cells/ml, n = 3 measurements of single-pass separation); and permeate; example cell concentration 0.91×10^6 cells/ml (range 0.83–1.0×10^6 cells/ml, n = 3 measurements of single-pass separation). Overall loss of cell number (based on total cell balance) in this scenario was less than 9% (total cells in feed: 5.7–6.1×10^6; total cells in retentate: 3.5–4.35×10^6; total cells in permeate: 1.6–1.75×10^6; overall balance >91%).

In this case, we measured for enrichment of osteoblastic lineages by assessing depletion of hESCs. Calculating the percentage of cells expressing pluripotency marker TRA-1-60 in feed (for example, day 11, percentage hESCs 44.9% ± 5.4%, n = 3 from a single-pass separation) and retentate (for example, day 11, percentage hESCs 30.4% ± 1.4%, n = 3 from a single-pass separation), we observed that the level of enrichment of stiffer osteoblastic (calculated as level of depletion of hESCs in the same manner as described earlier) cells in the retentate sample increases with increasing CEM (i.e., increased stiffness) of the differentiating cells during the first 15 days (Fig. 5); (for example, day 11, enrichment in osteoblastic cells of 32.2% ± 6.8%, n = 3 from single-pass separation), suggesting that the device is using stiffness as the main separation parameter.

DISCUSSION

The present study defines differences in the stiffness between pluripotent human embryonic stem cells and derivative mesenchymal and terminally differentiated osteoblast-like cells and dermal fibroblasts, based on atomic force microscopy measurements. This information was exploited to develop a cell separation device containing a woven mesh, employing tangential flow filtration separation principles. The device allowed for rapid yet gentle, label-free, and

scalable passive cell selection, prospectively amenable to automatable and high-throughput cell purification to meet future industrial and clinical demands for human pluripotent stem cell based advanced therapy medicinal products.

The growth and differentiation potential of human stem cells make them a promising source of cells for regenerative medicine. The development of effective and economical systems to select or purify pluripotent stem cells and derivatives thereof in ways that are reproducible, free of operator biases, non- or minimally invasive (including label-free), rapid, and scalable will ultimately dictate the extent of human pluripotent stem cell-based applications in regenerative medicine cell therapy. Currently, mammalian cell purification largely depends on binding of cell surface ligands as applied in fluorescent-activated flow cytometric- or magnetic-bead based sorting. However, these methods rely on knowledge about ligand expression, and subsequent availability and specificity of complementary probes, as well as on skilled personnel. In addition, probes will remain in the sample and probably even associated with the cell after segregation, potentially affecting cell state, with unknown consequences for the patient who will receive the cell preparation. Finally, as these platforms sort on a cell-by-cell basis in a fluid flow or column of limited cross dimensions, which limits the throughput and therefore the scalability of the techniques, these ligand-recognising selection methods in their current form do not provide automated, scalable strategies for stem cell purification. The device used in the current study constituted a prototype suitable for separation of cells for analysis with further work required to incorporate and validate design features to assure maintenance of sterility so that separated cells can be subsequently cultivated or used for industrial or therapeutic applications. Ideally, such a device would be "closed" to the external environment and constructed as an affordable single use disposable product.

Cell separation based on cell biophysical properties like size, shape, surface charge, and cell stiffness is still comparatively underexplored. Reports describing separation of various cell types based on their stiffness have been produced mainly in the fields of infectious diseases and cancer research and diagnostics. For example, recent papers describe microfluidics methods to separate healthy red blood cells from diseased ones (e.g., sickle cell anaemia (Kose *et al.*, 2009) and malaria infection (Hou *et al.*, 2010)), and benign from cancerous cells (e.g., breast cancer (Hou *et al.*, 2009), circulating tumour cells from blood (Hur *et al.*, 2011), and epithelial cancer cells mixed with white blood cells (Wang *et al.*, 2013)). Recently, we suggested that stiffness could also serve as the basis of a simple and efficient purification technique to discriminate subpopulations of hESC (Kiss *et al.*, 2011). Using AFM, we and others have previously demonstrated effective measurements of cell stiffness for a variety of cell types, including human embryonic (Kiss *et al.*, 2011), mouse embryonic (Pillarisetti *et al.*, 2011), and adult mesenchymal stem cells (Bongiorno *et al.*, 2014), and a variety of human cell lines (Wang *et al.*, 2013), and we applied this tool in our current study as well. We defined cell stiffness as CEM, which varies depending on the cell's function, fate, and lineage commitment. CEM is primarily determined by the presence, number, and distribution of specific organelles (e.g., nucleus and mitochondria) and the character and organisation of cytoskeletal elements (e.g., microfilaments, microtubules, and intermediate filaments) (Becker and Gard, 2006 and Yoon *et al.*, 2002). Thus, parameters for isolation of different cell types, for example, chondrocytes (stiff; high CEM) and fibroblasts (less stiff; lower CEM) will differ widely (Butt *et al.*, 2005). Similarly, metastatic cancer cells are softer than their "parental" cell type, likely to allow deformation and subsequent extravasation (Cross *et al.*, 2007 and Remmerbach *et al.*, 2009), supporting the notion that changes in stiffness likely reflect physiological adaptation for specific tasks, in this case enhanced migration through tissues. Cell stiffness can also change significantly during cell differentiation, as we report herein for osteogenic derivatives of stem cells, and as has previously been shown for a variety of cell types, including stem cells, myocytes, and myeloid cells by us (Kiss *et al.*, 2011) and others (Bongiorno *et al.*, 2014; Collinsworth *et al.*, 2002, Ekpenyong *et al.*, 2012; Pillarisetti *et al.*, 2011; Titushkin and Cho, 2007, Yourek *et al.*, 2007, and Yu *et al.*, 2010), with undifferentiated cells being softer (i.e., having a lower CEM) than their differentiated progeny. Indeed, mechanical property of cells has been proposed as a marker of differentiation state for stem cells (Darling *et al.*, 2008 and Kiss *et al.*, 2011).

Moreover, cell stiffness has recently been proposed as a predictive marker for multipotency and differentiation potential of adipose-derived stem cell clones (Gonzalez-Cruz *et al.*, 2012) and bone-marrow-derived mesenchymal stromal cells (Lee *et al.*, 2014).

We recently reported on the design and fabrication of a robust microfluidics device capable of separating a heterogeneous population of cells with variable degree of stiffness into enriched populations (Choudhury *et al.*, 2012). Here, we describe a mesh-based label-free TFF cell separation device where the level of enrichment of soft, pluripotent hESCs in a mixed cell population made up of hESCs and derivative osteolineage cells correlated with the stiffness of the differentiating derivatives. Thus, the stiffer the progeny cells, the more effectively they were separated from the softer progenitors in the feed population after a single pass through the device. These data strongly suggest that the device is using cell stiffness as a major separation parameter, and that differentiation-induced cell stiffness can form the basis of an efficient, label-free device for the separation of stem cells and their progeny. The data for day 21, however, deviated somewhat, with a relatively low enrichment percentage in spite of high median CEM. We hypothesize that this result is indicative of the biological process involved in the formation of osteoblastic lineages in cell culture plates. On both day 11 and day 21, a clear bimodal distribution of elastic modulus can be seen in Fig. 4. On day 11, we postulate this is because the population contains a number of stiffer cells (similar to those at day 6) and a number of softer cells (similar to those at day 15). However, we do not think that the cells are becoming stiffer again on day 21. Rather, we postulate that while the majority of cells are soft (as those at day 15), extensive mineralisation surrounding the cells biases the AFM measurements causing the cells to appear stiffer than they truly are. In suspension, however, a degree of dissociation between the cells and the mineralization is likely to occur, releasing a cell population which is in fact softer than the AFM data indicate. Consequently, a less efficient separation from the similarly soft hESCs, and thus a lower enrichment, is achieved.

This variation in elastic modulus and separation efficiency during the differentiation process emphasizes an important point regarding manufacture of cell therapy products. Purification should not necessarily be considered as an "end-of-process" operation to obtain the desired differentiated product, but rather be informed by the changing biophysical properties evidently occurring during the course of the differentiation process. Combined with the fact that the contaminating cells of most concern are those that do not differentiate but remain pluripotent, it may be beneficial to preferentially select for a cell type mid-way through a production process, when physical properties of targets and contaminants differ to the highest degree, and then allow the differentiation to continue post-selection.

Our study has not discriminated the relative contributions of other biophysical parameters such as cell size, shape, and charge with the potential to impact on separation efficiency in addition to cell deformability, although our flow cytometry results do clearly show that cell size is not a key separation factor. By using membrane pore cut-off sizes smaller than the minimum diameter of any cell in the system, we sought to reduce the prospective contribution of cell size and shape as cell separation parameters. Furthermore, on day 15, where the larger osteoblastic cells and the smaller hESCs have comparable median CEM, hardly any enrichment was observed, suggesting that size effects may not dominate elasticity effects. However, given the broad and overlapping CEM distribution profiles assessed by AFM in our study, most probably reflecting cellular heterogeneity resulting from spontaneous or asynchronous differentiation, it may be necessary to incorporate other separation parameters, such as charge, shape, and size, in order to efficiently discriminate different cell types.

The device demonstrated here is a first-pass proof-of-principle device and accordingly is not optimized for fluid mechanic effects. A volumetric flux of 0.4 ml/min through a membrane area of 1.4 cm^2 represents an average flux rate of approximately 170 l/m^2h, which is relatively low for such a large pore size of membrane and could clearly be improved. Similarly, whilst no measurement of pressure drop across the membrane could be taken in the current device design, pressure drop can be estimated after the fact from flux rates using a modified Hagen-Poiseulle equation as shown below

$$J = \frac{\Delta P d^2 \varepsilon}{32 x \mu},$$

where J is the volumetric flux, ΔP is the pressure drop, d is the pore diameter, ε is the relative porosity of the membrane, x is the pore length (in this case membrane thickness), and μ is the fluid viscosity. Operating conditions used during the experimental work presented here indicate an average pressure drop across the membrane around 1 Pa (calculated from the above formula), again very low for a filter of any kind.

The relatively low liquid flowrates chosen result in sub-optimal liquid velocities for mixing, and accordingly result in low Reynolds numbers. However, given the sensitivity of the target cells, flow conditions that minimize shear are crucial. A balance must be achieved between low shear and improved mixing. Given the low Reynolds numbers seen here it is very likely that, as the cells passing above the membrane will be constrained by streamline flow, many will not pass close to the membrane thus limiting the efficiency of separation per pass. Improving the flow patterns in the device to increase relative cell/membrane interaction, increase membrane driving force (pressure drop), and therefore increase flux should improve the level of separation per pass and hence the efficiency of the device, but this optimisation must be carried out in conjunction with computational fluid dynamic analysis and shear studies to ensure cell viability. This optimisation forms a separate body of future work, and the data here are presented simply to demonstrate the potential of separation via elastic properties. Though the data presented here are based on a non-optimised device, it is nevertheless clear that, with levels of removal approaching 50% in a single pass, our device represents a promising method for label-free purification of cells for clinical applications. The current device was run with a relative 3:1 volumetric flow rate ratio in favour if the retentate over the permeate, resulting in a reduction in total permeate cell numbers in the permeate relative to volumetric flow. Coupled with the reduced permeate flow rate, total numbers of cells in the permeate are around 5–10 fold lower than those in the retentate. This indicates that, whilst the device is effective at specific selection under these conditions, resulting in enriched permeate populations, both the selectivity and the overall flux of cells through the membrane could be optimized further to produce purer retentate and permeate populations and, potentially more crucially, an improved permeate yield if required through increased permeate flow rate. Separation performance of the device will be affected by a number of factors above and beyond hydrodynamic flow effects, including relative cell concentrations in the feed population and the mesh pore size in relation of the separated species. Improving the level of separation achieved in a single pass will be a key design improvement for moving from the proof-of-principle shown here to a more commercially relevant separation device. Further investigation of effects of pore size and cell type ratios in feed (containing an order of magnitude fewer pluripotent cells than our model systems) along with optimization of turbulence and pressure driving force, shear levels, residence time, and fluid flow conditions represent the next stage in the engineering design of this unit operation.

Within the current device design, it is highly likely that recycling (multiple pass separation) would improve the level of separation, however given the relative lack of understanding of the hydrodynamic environment it would unwise to speculate on the possible level of improved enrichment in this scenario. Rather, our future focus is on optimising single pass enrichment before considering recycling/multiple pass scenarios.

Some other filter-based label-free separation systems record higher purity levels, e.g., close to 99% for leukocyte depletion using normal flow filtration (NFF) (Sethu *et al.*, 2006) and >95% for red blood cell removal using TFF (Chen *et al.*, 2008), though the latter required rigorous sample dilution. In a direct comparison of NFF, TFF, and Weir- and Pillar-based flow filtration for sorting human blood, TFF outperformed the other three filter systems by showing an average efficiency of >70%–80% of trapping white blood cells and passing red blood cells (Ji *et al.*, 2008). Recently, Li *et al.* (2014) developed a cell sorting chip for processing whole blood, combining TFF with a microfiltration membrane, that could recover 27% of white blood cells with 94% purity. Using a dielectrophoresis-based device for separation of stem cells and

their differentiation progeny (osteoblasts), Song *et al.* (2015) achieved a collection efficiency of up to 92% and 67% for stem cells and osteoblasts, with a purity of up to 84% and 87%, respectively. Reported separation devices for human cell separation, however, focus on low-throughput applications, typically performing in the μl/min (Ji *et al.*, 2008; Sethu *et al.*, 2006; and Song *et al.*, 2015) to ml/h range (Li *et al.*, 2014 and Zhang *et al.*, 2012) and depending on the underlying methodology, may encounter scaling difficulties. Our device was able to maintain a permeate flow rate of 0.4 ml/min and process in the order of 5×10^6 cells/min through an effective separation area of only 1.4 cm^2. Since the principle behind our device described herein is broadly similar to TFF, a unit operation which is routinely scaled up for industrial applications including culturing bacterial, insect, and antibody-producing mammalian cells (van Reis and Zydney, 2001 and Reynolds *et al.*, 2003), scalability is not envisaged to be a hurdle for our device. Specifically, given that larger scale commercially available TFF unit cassettes can be 10 m^2 in membrane area or higher, and that TFF separation scales are reasonably predictable with increasing membrane surface area, it is entirely reasonable to assume that our technique, with optimisation of flow parameters within larger scale membrane devices, would be able to scale up to permeate flow rates of several tens of litres per minute and process cell numbers well in excess of 10^{11} cells/min.

In conclusion, we have designed and validated a novel device permitting the physical separation of undifferentiated and differentiating/differentiated human embryonic stem cells based on their stiffness. In the future, the evolution of this technology should benefit the purification of stem cells and their derivatives. This should improve the efficiency and safety of industrial and therapeutic applications that require them.

ACKNOWLEDGMENTS

This work has in part been funded by the Bioprocessing Research Industry Club (BRIC; BBSRC) Grant No. BB/G010323/1. Dr. Hoeve, Dr. De Sousa, and Dr. Willoughby gratefully acknowledge the BBSRC for their Flexible Interchange Programme Award (BB/L004925/1). We would like to thank L. Paterson and A. Kar for helpful discussions.

Becker, B. and Gard, D., "Visualization of the cytoskeleton in Xenopus oocytes and eggs by confocal immunofluorescence microscopy," Methods Mol. Biol. **322**, 69–86 (2006).

Bhagat, A., Bow, H., Hou, H. W., Tan, S. J., Han, J., and Lim, C. T., "Microfluidics for cell separation," Med. Biol. Comput. **48**(10), 999–1014 (2010).

Bongiorno, T., Kazlow, J., Mezencev, R., Griffiths, S., Olivares-Navarrete, R., McDonald, J. F., Schwartz, Z., Boyan, B. D., McDevitt, T. C., and Sulchek, T., "Mechanical stiffness as an improved single-cell indicator of osteoblastic human mesenchymal stem cell differentiation," J. Biomech. **47**(9), 2197–2204 (2014).

Butt, H. J., Cappella, B., and Kappl, M., "Force measurements with the atomic force microscope: Technique, interpretation and applications," Surf. Sci. Rep. **59**(1–6), 1–152 (2005).

Chen, X., Fu, D., Liu, C., and Li, H., "Microfluidic chip for blood cell separation and collection based on crossflow filtration," Sens. Actuators B **130**, 216–221 (2008).

Choudhury, D., Ramsay, W. T., Kiss, R., Willoughby, N. A., Paterson, L., and Kar, A. K., "A 3D mammalian cell separator biochip," Lab Chip **12**(5), 948–953 (2012).

Collinsworth, A. M., Zhang, S., Kraus, W. E., and Truskey, G. A., "Apparent elastic modulus and hysteresis of skeletal muscle cells throughout differentiation," Am. J. Physiol. Cell Physiol. **283**(4), C1219–1227 (2002).

Cross, S. E., Jin, Y. S., Rao, J., and Gimzewski, J. K., "Nanomechanical analysis of cells from cancer patients," Nat. Nanotechnol. **2**(12), 780–783 (2007).

Darling, E. M. and Di Carlo, D., "High-throughput assessment of cellular mechanical properties," Annu. Rev. Biomed. Eng. **17**, 35–62 (2015).

Darling, E. M., Topel, M., Zauscher, S., Vail, T. P., and Guilak, F., "Viscoelastic properties of human mesenchymally-derived stem cells and primary osteoblasts, chondrocytes, and adipocytes," J. Biochem. **41**(2), 454–464 (2008).

De Sousa, G. R., U.S. patent 8,100,400 (3 March, 2006).

Ekpenyong, A. E., Whyte, G., Chalut, K., Pagliara, S., Lautenschlager, F., Fiddler, C., Paschke, S., Keyser, U. F., Chilvers, E. R., and Guck, J., "Viscoelastic properties of differentiating blood cells are fate- and function-dependent," PLoS One **7**(9), e45237 (2012).

Gerrard, L., Zhao, D., Clark, A. J., and Cui, W., "Stably transfected human embryonic stem cell clones express OCT4-specific green fluorescent protein and maintain self-renewal and pluripotency," Stem Cells **23**(1), 124–133 (2005).

Gonzalez-Cruz, R. D., Fonseca, V. C., and Darling, E. M., "Cellular mechanical properties reflect the differentiation potential of adipose-derived mesenchymal stem cells," Proc. Natl. Acad. Sci. U.S.A. **109**(24), E1523–E1529 (2012).

Gonzalez-Gonzalez, M., Vazquez-Villegas, P., Garcia-Salinas, C., and Rito-Palomares, M., "Current strategies and challenges for the purification of stem cells," J. Chem. Technol. Biotechnol. **87**, 2–10 (2012).

Harkness, L., Mahmood, A., Ditzel, N., Abdallah, B. M., Nygaard, J. V., and Kassem, M., "Selective isolation and differentiation of a stromal population of human embryonic stem cells with osteogenic potential," Bone **48**(2), 231–241 (2011).
Hertz, H. and Angew, J., "Ueber die Berührung fester elastischer Körper," J. Angew. Math. **92**, 156–171 (1881).
Hou, H. W., Li, Q. S., Lee, G. Y. H., Kumar, P., Ong, C. N., and Lim, C. T., "Deformability study of breast cancer cells using microfluidics," Biomed Microdevices **11**(3), 557–564 (2009).
Hou, H. W., Bhagat, A. A., Chong, A. G., Mao, P., Tan, K. S., Han, J., and Lim, C. T., "Deformability based cell margination—A simple microfluidic design for malaria-infected erythrocyte separation," Lab Chip **10**(19), 2605–2613 (2010).
Hur, S. C., Henderson-Maclennan, N. K., McCabe, E. R. B., and Di Carlio, D., "Deformability-based cell classification and enrichment using inertial microfluidics," Lab Chip **11**, 912–920 (2011).
Ji, H. M., Samper, V., Chen, Y., Heng, C. K., Lim, T. M., and Yobas, L., "Silicon-based microfilters for whole blood cell separation," Biomed. Microdevices **10**(2), 251–257 (2008).
Kahler, D. J., Ahmad, F. S., Ritz, A., Hua, H., Moroziewicz, D. N., Sproul, A. A., Dusenberry, C. R., Shang, L., Paull, D., Zimmer, M., Weiss, K. A., Egli, D., and Noggle, S. A., "Improved methods for reprogramming human dermal fibroblasts using fluorescence activated cell sorting," PLoS One **8**, e59867 (2013).
Kiss, R., Bock, H., Pells, S., Canetta, E., Adya, A. K., Moore, A. J., De Sousa, P., and Willoughby, N. A., "Elasticity of human embryonic stem cells as determined by atomic force microscopy," J. Biomech. Eng. **133**(10), 101009 (2011).
Kose, A. E., Fischer, B., Mao, L., and Koser, H., "Label-free cellular manipulation and sorting via biocompatible ferrofluids," Proc. Natl. Acad. Sci. U.S.A. **106**(51), 21478–21483 (2009).
Kunze, A., Che, J., Karimi, A., and Di Carlo, D., "Research highlights: Cell separation at the bench and beyond," Lab Chip **15**(3), 605–609 (2015).
Kuznetsova, T. G., Starodubtseva, M. N., Yegorenkov, N. I., Chizhik, S. A., and Zhdanov, R. I., "Atomic force microscopy probing of cell elasticity," Micron **38**(8), 824–833 (2007).
Lee, C. L., Shi, H., Poon, Z., Nyan, L. M., Kaushik, T., Shivashankar, G. V., Chan, J. K. Y., Lim, C. T., Han, J., and Van Vliet K. J., "Multivariate biophysical markers predictive of mesenchymal stromal cell multipotency," Proc. Natl. Acad. Sci. U.S.A. **111**(42), E4409–E4418 (2014).
Li, X., Chen, W., Liu, G., Lu, W., and Fu, J., "Continuous flow microfluidic blood cell sorting for unprocessed whole blood using surface micromachined microfiltration membranes," Lab Chip **14**, 2565–2575 (2014).
Pillarisetti, A., Desai, J. P., Ladjal, H., Schiffmacher, A., Ferreira, A., and Keefer, C. L., "Mechanical phenotyping of mouse embryonic stem cells: Increase in stiffness with differentiation," Cell. Reprogram. **13**(4), 371–380 (2011).
Radmacher, M., Tillmann, R. W., Fritz, M., and Gaub, H. E., "From molecules to cells: Imaging soft samples with the atomic force microscope," Science **257**(5078), 1900–1905 (1992).
Remmerbach, T. W., Wottawah, F., Dietrich, J., Lincoln, B., Wittekind, C., and Guck, J., "Oral cancer diagnosis by mechanical phenotyping," Cancer Res. **69**(5), 1728–1732 (2009).
Reynolds, T., Boychyn, M., Sanderson, T., Bulmer, M., More, J., and Hoare, M., "Scale-down of continuous filtration for rapid bioprocess design: Recovery and dewatering of protein precipitate suspensions," Biotechnol. Bioeng. **83**(4), 454–64 (2003).
See supplementary material at http://dx.doi.org/10.1063/1.4939946 for detailed description of atomic force microscopy procedures and data analysis algorithms and further details of our previously published microchannel separation device, along with legends for Figures S1 and S2 and for Figure S1 (CEM probability distributions of H1-MPs undergoing osteogenesis) and Figure S2 (Microchannel Separation Device (MSD) design).
Sethu, P., Sin, A., and Toner, M., "Microfluidic diffusive filter for apheresis (leukapheresis)," Lab Chip **6**(1), 83–89 (2006).
Song, H., Rosano, J. M., Wang, Y., Garson, C. J., Prabhakarpandian, B., Pant, K., Klarmann, G. J., Perantoni, A., Alvarez, L. M., and Lai, E., "Continuous-flow sorting of stem cells and differentiation products based on dielectrophoresis," Lab Chip **15**(5), 1320–1328 (2015).
Sottile, V., Thomson, A., and McWhir, J., "*In vitro* osteogenic differentiation of human ES cells," Cloning Stem Cells **5**(2), 149–155 (2003).
Titushkin, I. and Cho, M., "Modulation of cellular mechanics during osteogenic differentiation of human mesenchymal stem cells," Biophys. J. **93**(10), 3693–3702 (2007).
van Reis, R. and Zydney, A., "Membrane separations in biotechnology," Curr. Opin. Biotechnol. **12**(2), 208–211 (2001).
Velugotla, S., Pells, S., Mjoseng, H. K., Duffy, C. R., Smith, S., De Sousa, P., and Pethig, R., "Dielectrophoresis based discrimination of human embryonic stem cells from differentiating derivatives," Biomicrofluidics **6**(4), 44113 (2012).
Wang, G., Mao, W., Byler, R., Patel, K., Henegar, C., Alexeev, A., and Sulchek, T., "Stiffness dependent separation of cells in a microfluidic device," PLoS One **8**(10), e75901 (2013).
Yoon, Y., Pitts, K., and McNiven, M., "Studying cytoskeletal dynamics in living cells using green fluorescent protein," Mol. Biotechnol. **21**(3), 241–250 (2002).
Yourek, G., Hussain, M. A., and Mao, J. J., "Cytoskeletal changes of mesenchymal stem cells during differentiation," ASAIO **53**(2), 219–228 (2007).
Yu, H., Tay, C. Y., Leong, W. S., Tan, S. C., Liao, K., and Tan, L. P., "Mechanical behavior of human mesenchymal stem cells during adipogenic and osteogenic differentiation," Biochem. Biophys. Res. Commun. **393**(1), 150–155 (2010).
Zhang, W., Kai, K., Choi, D. S., Iwamoto, T., Nguyen, Y. H., Wong, H., Landis, M. D., Ueno, N. T., Chang, J., and Qin, L., "Microfluidics separation reveals the stem-cell-like deformability of tumor-initiating cells," Proc. Natl. Acad. Sci. U.S.A. **109**(46), 18707–18712 (2012).